WFC3 Instrument Science Report 2011-18

First Results from Contamination Monitoring with the WFC3 UVIS G280 Grism

B. Rothberg, N. Pirzkal, S. Baggett
November 2, 2011

ABSTRACT

The presence of contaminants within the optical light path of the instrument or telescope can alter photometric zeropoints and the observed flux levels of imaging and spectra, particularly at UV wavelengths. Regular monitoring of a spectro-photometric standard star using photometric filters has been used in the past to monitor the presence of contaminants and (when necessary) re-calibrate zeropoints. However, the use of the WFC3 UVIS Grism mode (G280 filter) may provide a more robust early alert detection system for the presence of contaminants, in particular, those that are photo-polymerized from the bright Earth. These contaminants may collect on surfaces in the optical light path of the telescope. The G280 grism is sensitive to light at wavelengths below the cutoff of the bluest UV filter (F218W). In this ISR, we present: 1) the first results from G280 monitoring for the period of 2010-November through 2011-August; 2) the discovery of an anomaly in the WCS header information of sub-array exposures; and 3) an outline for reducing standard G280 grism observations and the specialized case of observations obtained in sub-array mode.

Introduction

Analysis of both WF/PC-1 and WFPC2 instruments post-flight showed evidence of contamination from layers of polymerized contaminants (e.g. McMaster et al. 2002, Lim et al. 2010a, Lim et al. 2010b). The contaminants produced a detectable drop in the measured flux levels for filters at the shortest wavelengths. For example, a 20-25% drop in transmission was detected in the F122M filter (Lim et al. 2010a), while Gonzaga & Biretta (2009) noted the presence of "worms" caused by a thin contaminant on the CCD windows in flats from 1994-

1995. Such contaminants may also be found on the pickoff mirror located in the HST hub area. The G280 grism filter in WFC3 has the potential to detect the presence of such contaminants before they are detected in the shortest wavelength imaging filter (F218W) because it probes even shorter wavelengths, where the effects of contamination will be larger. These effects increase over time. Those that are localized to the CCD window can be corrected by decontamination (decon) which is a process by which the camera heads are warmed causing the evaporation of the contaminants from the faceplate. However, if these contaminants lie on the pickoff mirror, then a decon will have no effect. Program 12333, a monitoring program whose goal is to assess the relative throughput stability to 1% in the UV and 2% in the IR, also includes a component which monitors the flux through the G280 grism filter. This ISR presents the first results for this monitoring program and establishes a methodology for assessing changes in the flux levels and comparing those directly with other filters. This methodology will be applied to future visits in Cycle 18 and Cycle 19 to monitor the instrument and telescope for the presence of UV contaminants.

Observations

The results presented in this report are based on observations from the ongoing Cycle 18 calibration program 12333 (PI: Baggett) of the spectrophotometric star GRW+70d5824. Two orbits are executed every five weeks. The start date was 17 November, 2010. This gives a baseline of 10 months. The grism sub-program consists of one direct image of the star taken with the F300X filter in full-frame ACCUM mode (exposure time of 1.0 second), and two exposures (40.0 seconds each) taken with the G280 filter (grism) using ACCUM and the sub-array mode: SIZEAXIS2=768; CENTERAXIS2=1026; AMP=D. The two grism exposures were dithered using the WFC3-UVIS-DITHER-LINE pattern. This pattern uses a two-point scheme in which the second exposure is offset relative to the first with a POS TARG X of +0.099 arcsec and a POS TARG Y of +0.106 arcsec. This translates into a dither of +2.5 pixels in both the X and Y axes in the reference frame of the array.

The observation scheme for the grism sub-program was changed between Visit 6 and Visit 7. For Visits 1-6, the aperture selected for the direct image was the G280-REF with no POS TARG offset. This produced a direct image in which the star was placed on CHIP1 of the UVIS array. The UVIS-REF aperture was used for the two G280 exposures along with a POS TARG offset of 0.0, -50.0. This yielded G280 exposures in which the star was on the center of CHIP2 of the UVIS array. In Visits 7-9, the F300X direct image of the star was changed to include a POS TARG offset of 0.0, -50.0. This placed the star at the center of CHIP2 in the direct image.

Data Analysis

Reduction of G280 Grism Data

A standard G280 grism reduction method uses a direct image to generate a catalog of objects. Nominally, the direct image is first processed with MULTIDRIZZLE to create a new image. This takes the FLT file as input and produces a new DRZ (drizzled) file which combines CHIP1 and CHIP2 and corrects for geometric distortion. Next, SEXTRACTOR (or any similar detection program) is used to identify the X and Y coordinates of all objects on the DRZ direct image. This catalog is used by the task AXECORE in the reduction software aXe (Pirzkal et al. 2003, Kümmel et al. 2009) to compute the positions of the spectra on CHIP1 and CHIP2 for the G280 exposures. The grism images, CHIP1 and CHIP2 are treated as separate "instruments" by aXe.

Detection of an Anomaly in Sub-array Exposures

The reduction of the grism sub-program data proved somewhat more complicated than the typical G280 grism process described above. The analysis was affected by the discovery of an anomaly in the World Coordinate System (WCS) information in the headers of the sub-array observations, but not present in the full frame observations. Dubbed the "Rothberg Sub-array Anomaly," (RSA) it is a mismatch between the WCS information in the full frame and sub-array observations. The WCS information for the grism exposures taken in sub-array mode were offset several arcminutes from the direct images taken in full-frame mode. This anomaly affected the creation of the object catalog.

The anomaly was not related to the CALWF3 calibration task, as the **.raw* images were found to suffer from this problem. A more detailed inspection of the issue indicated that the WCS subsystem code used in OPUS to load aperture information from the Science Instrument Aperture File (SIAF) was incorrectly identifying the observations as being centered on CHIP1. When a sub-array image was taken, the SIAF data corresponding to the reference aperture that was used would be loaded by OPUS, overriding all other considerations (POS TARGs, etc). Although a POS TARG was used to center the G280 (Visits 1-9) and F300X (Visits 6-9) exposures on CHIP2, the G280-REF and UVIS apertures were used. These apertures have their reference points on CHIP1. As a result, while the data were centered on CHIP2, they were processed by the WCS subsystem code in OPUS as if they were taken on CHIP1. A fix has been tested which will modify the WCS subsystem code by comparing the X corner value of the sub-array image with the chip number listed in the SIAF as the reference location for the aperture selected. If the code finds that the X corner indicates the exposure was on CHIP2, it will override the SIAF parameters and force it to use the values for CHIP2. This anomaly does not appear to affect pre-defined sub-array apertures, but appears to occur only when full-frame apertures (i.e. G280-REF and UVIS) are used with a sub-array exposure.

Modified Reduction of G280 Grism Data

In order to account for the various observational setups and the RSA, a slightly different method was used to reduce the G280 exposures. First, the sub-array exposures must be embedded within a full-frame image. This is a requirement for aXe to process the data. A python script, "*embed_subs.py*" developed by H. Bushouse was used to embed the sub-arrays in a full-frame image. The script can be used for UVIS or near-IR sub-arrays. Additional information can be found on the WFC3 Grism Resource Page: http://www.stsci.edu/hst/wfc3/analysis/grism_obs/wfc3-grism-resources.html.

An object catalog containing only the star GRW+70d5824 was generated manually. For Visits 1-6, the star was placed on CHIP1 for the direct image, not CHIP2. This setup, along with the RSA, required a catalog to contain pseudo-coordinates for the star, that is, coordinates for the star as if the direct image was centered on CHIP2. Due to the nature of the grism filters, spectra are offset spatially on the array from their direct image X and Y coordinates. In the case of the UVIS array, this offset varies as a function of position due to geometric distortion. The grism offset was determined for the center of the CHIP2 array using GO archive data from Cycle 17 (Program 11594, PI: O'Meara). Next, another catalog was created which incorporated the WFC3-UVIS-DITHER-LINE offset of +2.5 pixels in X and Y for the second grism exposure. For Visits 7-9, the X and Y coordinates of the star in the direct image (centered on CHIP2) were measured via centroiding with IMEXAMINE in IRAF. These coordinates were used for the catalog for the first grism exposure. The X and Y coordinates used in the catalog for the second grism exposure were offset by +2.5 pixels in X and Y to account for the WFC3-UVIS-DITHER-LINE.

The object catalog used by aXe nominally contains 12 columns (for additional information on the catalog files, please see the WFC3 Grism Frequently Asked Questions Webpage: http://www.stsci.edu/hst/wfc3/analysis/grism_obs/wfc3-grism-faq.html). The X and Y coordinates of the star in the direct image derived above were used in columns 2 and 3. Columns denoted with "WORLD" were set to values of NaN. The only task in aXe used to extract the spectra was AXECORE. The data were extracted with AXECORE using a vertical extraction method due to the extreme curvature of the orders. To force AXECORE to use a vertical extraction, the column THETA_IMAGE in the object catalog was to set to a value of "-90.0". Two keywords must also be set in AXECORE: `orient='yes' slitless_geom='no'`. A specific extraction aperture of 20 pixels in diameter was used. The aperture size was selected to be large enough to ensure that all of the flux is measured even if the trace or measured position of the +1 Order are imprecise. The extraction aperture that AXECORE uses is affected by the A_IMAGE, B_IMAGE, THETA_IMAGE columns in the object catalog and the keyword EXTRFWHM passed to the aXe task AXECORE. In the object catalogs the values used were: A_IMAGE=B_IMAGE = 5.0. The following AXECORE parameters were used:

```
axecore G280.lis WFC3.UVIS.CHIP2.conf extrfwhm=4.0 drzfwhm=0.0
back='no' backfwhm=0.0 orient='yes' slitless_geom='no'
cont_model='gauss' sampling='drizzle' adj_sens- weights+
inter_type="linear"
```

Additional details on these parameters can be found in the aXe manual. The configuration file "WFC3.UVIS.CHIP2.conf" used for the analysis is based on new G280 calibration information and will be available for public use shortly (Pirzkal et al. 2011). Revised calibrations for CHIP1 are currently scheduled for Cycle 19. Currently, the task AXEDRIZZLE does not support the UVIS G280 grism. The final spectra used for analysis were output from AXECORE.

Analysis

Intra-Visit Comparisons

Due to the non-standard methods used to obtain and reduce the data, the first step in the analysis was to assess whether the flux levels for intra-visit exposures were self-consistent. Figure 1 shows nine grey-scale, two-dimensional images of the ratio of exposure A to exposure B of the G280 spectra for each visit. The grey-scale is 0 to 2. Wavelength increases leftward. The UV areas of interest are X > 680 pixels. Figure 2 contains nine plots showing the ratio of counts in exposure A to exposure B for the extracted 1-dimensional spectra for each visit (with errors). At the shortest wavelengths there appears to be an offset for intra-visit comparisons. At $\lambda < 1600$ Å, the average offsets range from 7-27%; at $1600 \leq \lambda < 2200$ Å the average offsets range from 6-8%, and at $\lambda \geq 2200$ Å the average offsets range from 2-9%. Overall Visit 9 shows the largest intra-visit differences. The offsets are likely affected by two issues: 1) the extreme curvature of the orders (not just the +1 order) at the shorter ($\lambda < 2000$ Å) wavelengths produces larger uncertainties in the spectral trace; and 2) at wavelengths $\lesssim 1800$ Å the calibration still has large uncertainties. The revised spectral trace and wavelength calibrations for CHIP2 are limited. They are based on calibration observations of three positions on CHIP2. Improved wavelength calibration at shorter wavelengths for CHIP2 is currently being tested using high-resolution UV spectra of the calibrator WR-14 (Pirzkal et al. *in preparation*). New observations at multiple positions on CHIP1 and CHIP2 will be obtained in Cycle 19 calibration programs to improve wavelength calibration as a function of position on both chips.

Flux Comparison

In this section, we compare the fluxes from different orbits to look for variations as a function of time. As noted earlier, the CHIP2 configuration is flux calibrated only for $\lambda > 1900$ Å. The average of the data for the two G280 exposures taken in each orbit were used in these and subsequent comparisons. Figure 3 shows a comparison among the flux calibrated spectra for Visits 1-9 at $\lambda = 1900$-2300 Å. This range is displayed because it includes wavelengths shorter than the bluest filter available on WFC3 for imaging (F218W $\lambda_c = 2224$ Å, $\Delta\lambda = 322$ Å). Figure

3 *appears* to show an *increase* in flux with time at the shortest wavelengths ($\lambda \lesssim 2000$ Å). However, this change in flux does not appear to be at a statistically significant level for the most part. Relative to Visit 1, only 2 data points in Visit 9 ($\lambda \approx 1956$ Å, 1968 Å) are at least 3σ different. At the 2σ level there are differences for: Visit 7 at 1920 Å $\lesssim \lambda \lesssim$ 1991 Å; Visit 8 at 1909 Å $\lesssim \lambda \lesssim$ 1968 Å; and Visit 9 at 1909 Å $\lesssim \lambda \lesssim$ 1991 Å. Figure 4 shows the same comparison, but at longer wavelengths (2300 Å $< \lambda <$ 3500 Å), and no significant differences in flux as a function of time at the 2 or 3σ. This trend continues until the end of the extracted wavelength range.

Figure 5 re-plots Figure 3, but this time showing the fluxes in Visits 2-9 relative to Visit 1 for better visual comparison. The differences do appear to be systematically larger, however the trend with time remains unclear. The relative differences are +/-8% and still within the error bars (as noted above). This may suggest a trend, but longer baselines and refined calibrations are needed.

Native Count (e-/sec) Comparisons at $\lambda \leq 1900$ Å

Given the current limitations of the flux calibration at $\lambda \lesssim 1900$ Å for CHIP2, we next compared the native counts (units of e-/sec) for the extracted spectra between visits at these bluer wavelengths. A caveat to this comparison is that at the very shortest wavelengths the wavelength calibrations are quite uncertain ($\lambda \lesssim 1600$ Å), and the errors computed from the fluxes are significantly underestimated compared to the uncertainties from the spectral trace and wavelength calibrations. The uncertainties in trace and wavelength calibration are of concern here because the two exposures were obtained using a dither pattern, thus the actual positions of the spectra on the array are different by +2.5 pixels in X and Y. In future visits, the use of a CR-SPLIT will improve intra-orbit comparisons because the spectra in both exposures will be in the same position on the UVIS array.

Due to the noise in the data, we restrict the count comparisons to $\lambda > 1600$ Å (actual differences). Figure 6 shows a comparison of the relative fluxes for 1600 Å $< \lambda <$ 1900 Å, similar to the comparison shown in Figure 5. There are 3σ differences relative to Visit 1, but any systematic trends with time remain unclear. There is significant dispersion at the shortest wavelengths in Figure 6. At $\lambda \gtrsim 1800$ Å there is better convergence and smaller errors. Even here, it is not entirely clear that there is a systematic trend of increasing or decreasing flux *with* time. For example, Visit 9 trends below Visit 8, relative to Visit 1. If the contamination is on the CCD window, then decon will remove it periodically. If the contamination is elsewhere, then flux levels should *decrease* with time. Neither of these trends is shown here.

Comparisons in a Pseudo-bandpass and 5 WFC3 Filters

The final set of analysis can be directly compared to the photometric monitoring component of Program 12333. The fluxes from the G280 exposures have been convolved with filter transmission profiles for the F218W, F225W, F275W, F336W, and F438W filters for WFC3.

Using this, and the PHOTFLAM values from the WFC3 Handbook, the G280 fluxes have been converted to apparent AB magnitudes for direct comparison with the photometric observations. The aperture diameter used to extract the G280 spectra was 20 pixels. This aperture size is ideally suited for photometry of isolated stars and should not require any additional aperture corrections for direct comparisons. In addition to the five WFC3 filters, we have also used a pseudo-filter to monitor the response at wavelengths below the FWHM of the F218W. The bandpass for this pseudo-filter is 1900-2050 Å. The wavelength range was selected based on a qualitative judgment of the degree of uncertainty seen in the counts across Visits 1-9. The magnitude in this bandpass was computed by summing the average fluxes (from the two G280 exposures at each visit) between the filter endpoints, then dividing by $\Delta\lambda$ (=250 Å). This was then converted to a pseudo-magnitude by taking: -2.5 * Log_{10} (flux) + ZP, where ZP was chosen to be 25.0 (an arbitrary value). Figure 7 shows the 6 filter comparisons plotted against the Modified Julian Date (MJD) of the 9 visits. A linear least-squares (lsq) error-weighted fit was applied to the data to determine whether this method displayed any systematic trends. The fits are noted in each panel. As expected, the error bars in the 1900-2050 Å bandpass are significantly large (~ +/- 0.10 mag). While visually there is an upward (brightening) trend in this panel, it is not statistically significant. It is possible that with improved flux, wavelength, and spectral trace calibrations in this wavelength range that the trend will be confirmed in the future. As Program 12333 is continued for the remainder of Cycle 18 and Cycle 19 the broader baseline and refined methods of observing and analysis will clarify whether the weak trend seen at $\lambda <$ 2050 Å is real.

The remaining filters do not show any indications of a trend, either increasing or decreasing flux with time. Again, the errors as currently derived are ~+/-0.05 mag, which is somewhat larger compared to what can be achieved photometrically. However, it is likely that once improved calibrations are applied to this and future visits, the error bars will be shrink significantly. The strength of the method presented in this section is that these data can be compared directly to the photometric component of the program and compared with results from other instruments.

Additional Errors Introduced By Pixel Shifts

Finally, we attempt to address the impact of positional offsets in how they affect flux measurements. As noted above, the observations used a +2.5 X, +2.5 Y pixel offset between the two exposures within each orbit. That coupled with uncertainties introduced by having to manually derive the location of the star in the direct image adds to the errors in our analysis. As a test of how much offsets in pixel space can affect extracted flux and native counts (e-/sec), we extracted spectra from exposure A in Visit 7 multiple times, each time adding +/-0.5 pixels to the X and Y position in the catalog used by AXECORE to locate and extract a spectrum (e.g. creating a 3x3 grid around the center position). This gives 8 positions to test. Visit 7 was

selected because the star was observed with CHIP2 and we were able to locate its X and Y coordinates using IMEXAMINE in IRAF. Exposure A was used because there was no dither relative to the direct image. Thus, we know the "true" position of the star as AXECORE "sees" it and can test the effects on extracted spectra by introducing errors in the position. An offset of 0.5 pixels was selected based on the difficulties encountered in creating an object catalog for Visits 1-6 (e.g. determining the position of the 0th order in the G280 exposures and backtracking what the direct image coordinates should have been if CHIP2 were used). This offset represents a "worst-case" scenario to test.

The counts and fluxes were then compared relative to the counts and fluxes extracted from knowing the "true" position of the star. We are only interested in the bluest parts of the spectrum, so fluxes are compared for 1900 Å < λ < 2050 Å, and counts are compared for 1600 Å < λ < 1900 Å. Figure 8 shows these comparisons (fluxes *top*, counts *bottom*). For the flux calibrated spectra, the errors introduced by +/-0.5 pixels are ~ +/-5%. However, counts drop by as much as 30% until ~1750 Å, and then are ~5-10% lower than expected. The most pronounced effect on the flux comes from offsets in the X direction. In the Y direction, an offset of +/-0.5 pixels has a negligible effect on either flux or summed counts. This effect is shown in Figure 8. Different symbols and colors are used in the plot to make this effect clear. An offset of 0 pixels, +0.5 pixels, and -0.5 pixels in X produces three groups in Figure 8. Within those groups, the Y offset has a negligible effect.

Conclusions

We have presented the first results from UV monitoring of the health of the WFC3 instrument using the G280 grism filter. Rather than evidence of flux diminution over time, as had been seen in some filters in WFPC2, weak evidence is seen of an *increase* in flux over the 9 visits at λ < 2050 Å. Preliminary results from both COS and STIS at epochs earlier to the G280 data presented here show trends of an increase in flux with time at the bluest wavelengths. However, those results are still pending further analysis. While *visually* a similar trend appears in the G280 data, that trend cannot be supported statistically. The evidence presented for a flux increase is hampered by difficulties encountered in both the observations and analysis of the data. The sensitivity at λ ≤ 1900 Å (the current limit of flux calibration) is based on comparing the measured errors in e-/sec relative to e-/sec. In the pseudo-filter range (1900 Å < λ < 2050 Å), these errors are currently ~4-9% depending on wavelength. If the derived positions in X are wrong for Visits 1-6, or the dither pattern used in Visit 7-9 is not exactly +2.5 pix in X (due to telescope error), then even a 0.5 pixel mistake can produce additional errors of +/-5% in flux, and a loss of 5-10% in counts at the bluest wavelengths. Below this wavelength range, the errors become extremely large. However, what further complicates matters is the uncertainties introduced from the non-standard observing and reduction techniques employed. Again, once calibrations are improved, and the RSA is corrected for previous data, the errors should drop significantly.

As of Visit 10 and beyond, the observing program has been altered in two ways to ensure better uniformity and control over possible sources of error: 1) The F300X direct image and G280 exposures are obtained using sub-arrays; and 2) the WFC3-UVIS-DITHER-LINE has been replaced with a CR-SPLIT so that the telescope does not move during the F300X and the two G280 exposures. This will improve rejection of bad pixels and cosmic rays. More importantly, it will improve the spectral trace and wavelength calibration. This is because these calibrations are heavily dependent on the position of the spectra on the CCD. If the position does not change between exposures, the same calibration is valid for *both* positions, reducing uncertainties and errors from position changes (as has been shown to occur above). CR-SPLIT will not compensate for bad pixels, however, ignoring one or several bad pixels will not affect the overall program.

We have also documented the discovery of an unusual anomaly in the WCS headers of sub-array observations. A fix for this anomaly should be available soon and will be transparent to the user. However, any G280 and UVIS direct imaging data previously obtained from the archives, which employed the G280-ref or UVIS apertures in sub-array mode, will need to be re-downloaded.

The methods developed here for monitoring potential changes in flux at UV wavelengths, including those bluer than the F218W filter, will prove useful once the improved wavelength, trace and flux calibrations have been completed. While the errors are currently large, the methodology is sound. Once the Cycle 19 calibrations are completed, it is expected that the errors caused by changes in position (wavelength and trace calibration) and flux calibration will decrease significantly, yielding total errors within only 1-2% or better. The advantage of using the G280 grism filter over the F218W is that it is sensitive to wavelengths bluer than the F218W where the effects of contamination will be detected earlier. It should not replace the filter monitoring, however, because (as it has been demonstrated) one can compare the G280 directly with the filters as a sanity check.

Acknowledgments

We would like to thank Howard Bushouse for providing the python scripts for embedding the sub-array images within a full-frame and for invaluable assistance in determining the root cause the RSA. We would also like to thank Bryan Hilbert for work done in refining the spectral trace and wavelength calibration for the UVIS CHIP2 and Tomas Dahlen for reviewing the manuscript and providing helpful suggestions for improving this ISR.

References

Gonzaga, S. & Biretta, J. 2009, WFPC2 ISR 2009-02, "WFPC2 F343N Filter Throughput Decline."

Kümmel, M., Walsh, J.R., Pirzkal. N., Kuntschner, H. & Pasquali, A. 2009, PASP, 121, 875.

Lim, P.L., Quijada, M., Baggett, S., Biretta, J., Mackenty, J., & Boucarut, R., Rice. S., & del Hoyo, S. 2010a, The 2010 STScI Calibration Workshop, "WFPC2 Filters After 16 Years on Orbit."

Lim, P.L., Quijada, M., Baggett, S., Biretta, J., Mackenty, J., & Boucarut, R. 2010b, WFPC2 ISR 2010-05, "WFPC2 Filters After 16 Years On Orbit."

McMaster, M. & Whitmore, B. 2002, WFPC2 ISR 2002-07, "Updated Contamination Rates for WFPC2 UV Filters."

Pirzkal, N., Pasquali, A., & Demleitner, M. 2001, ST-ECF Newslett., 29, 5

Pirzkal, N., Hilbert, B., & Rothberg, B. 2011, WFC3 ISR "Wavelength and Spectral Trace Calibration of the UVIS Array." *in preparation*.

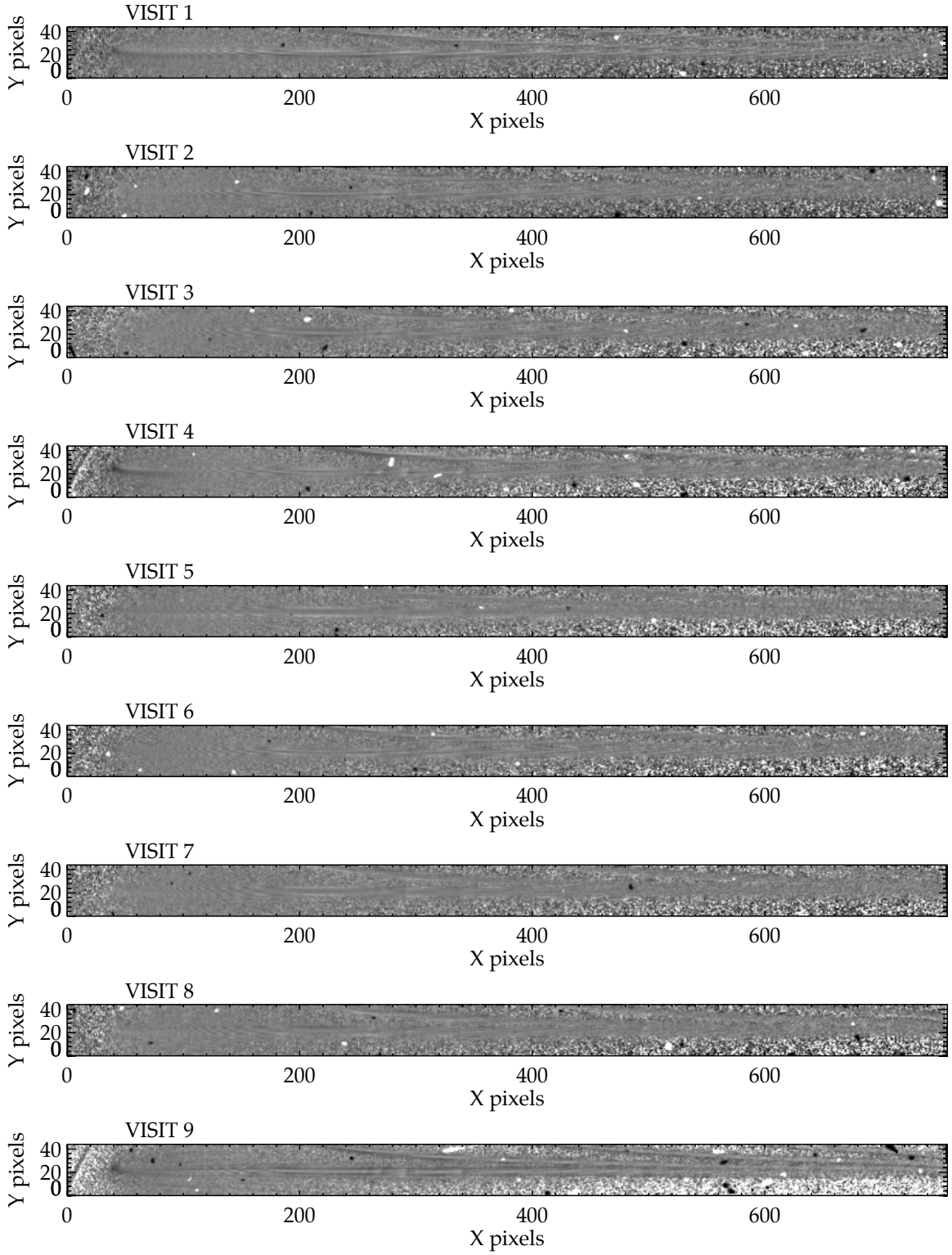

Figure 1 Grey-scale 2-dimensional images of the rectified G280 grism +1 Orders. Each panel shows the ratio of the two exposures taken in each visit. The grey-scale values range from 0 to 2.0. Wavelength increases leftward (ie. X pixel 1 is the longest wavelength).

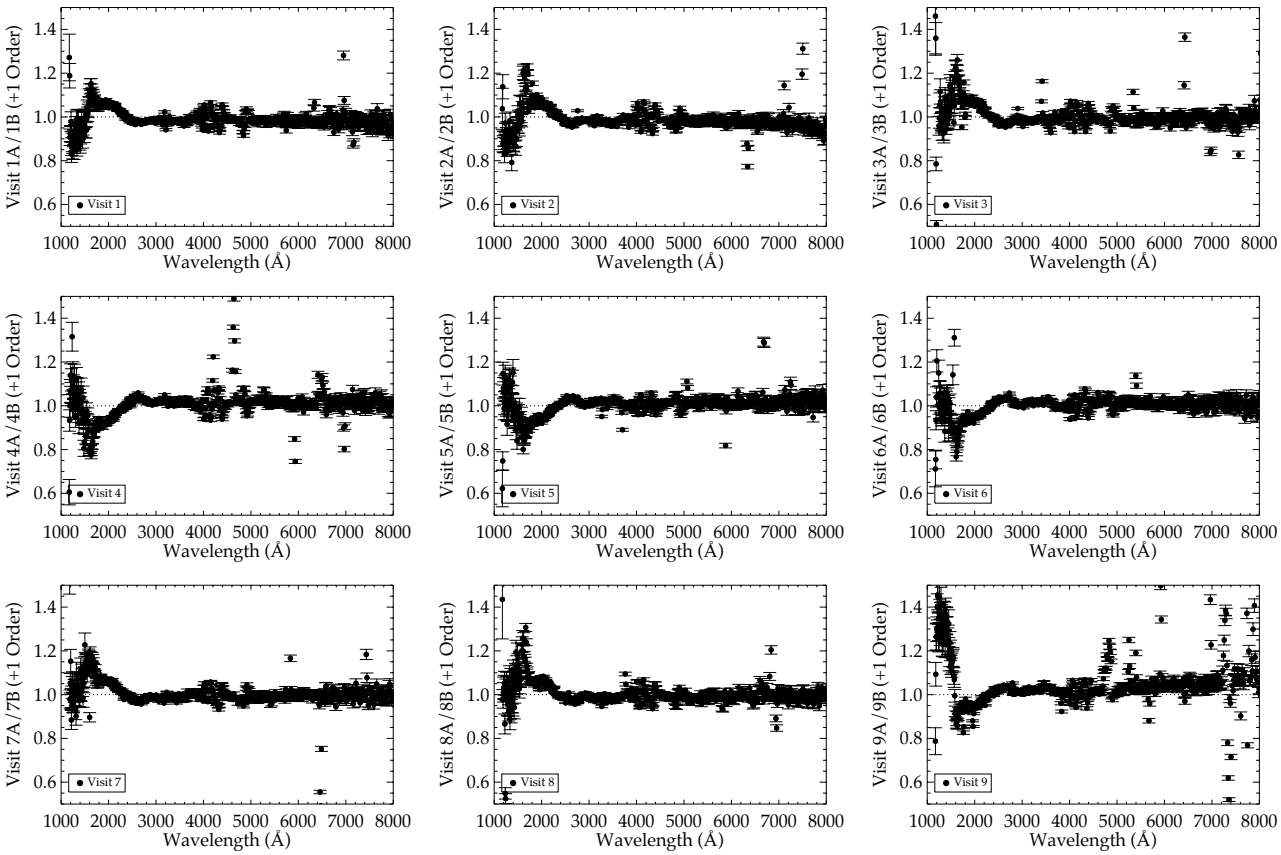

Figure 2: Each plot shows the ratio of the extracted spectra (exposure A/exposure B) for each visit. The spectra were extracted in an aperture of 20 pixels in diameter. Overplotted are the propagated flux errors. The large error bars at shorter wavelengths make these offsets appear worse in these plots compared to actual measured values. It should also be noted that Figure 2 compares counts, and not calibrated fluxes. The revised configuration file for CHIP2 is flux calibrated for the +1 Order only, and only at $\lambda > 1900$ Å.

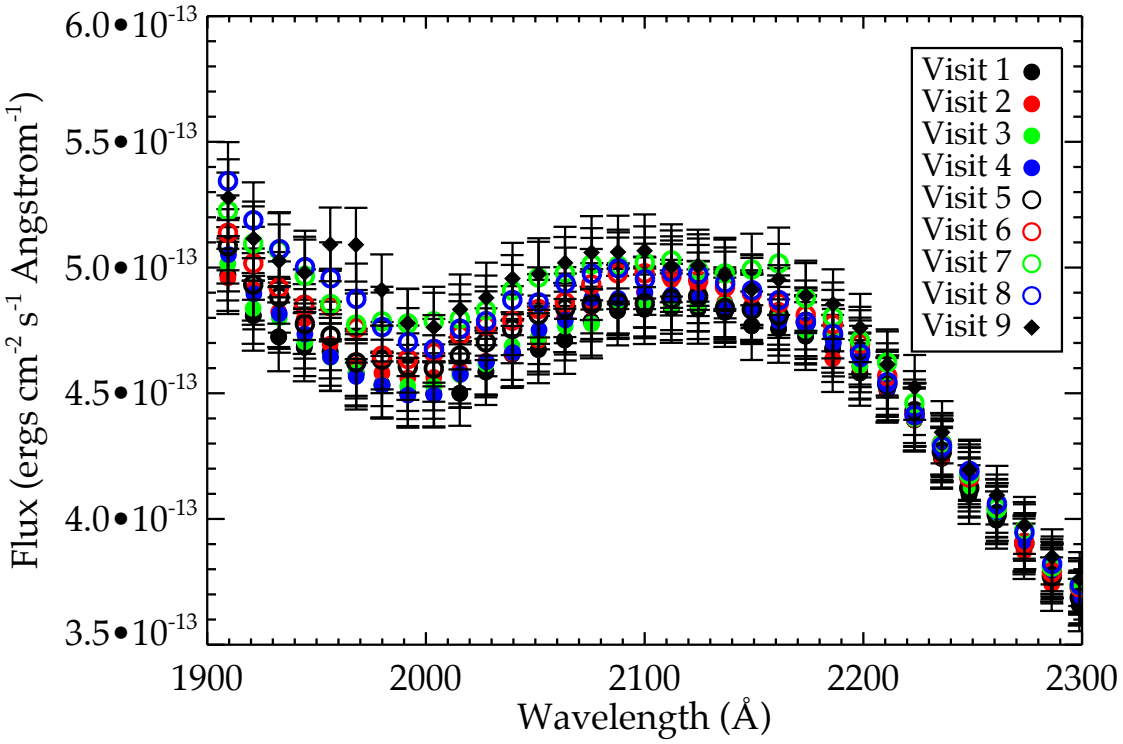

Figure 3: The fluxes for Visits 1-9 are shown for the bluest wavelength range currently flux calibrated. The plot shows some variation between visits at λ < 2000 Å, but it is unclear if this is time-dependent because data from Visit 1 does not always show the smallest or largest flux.

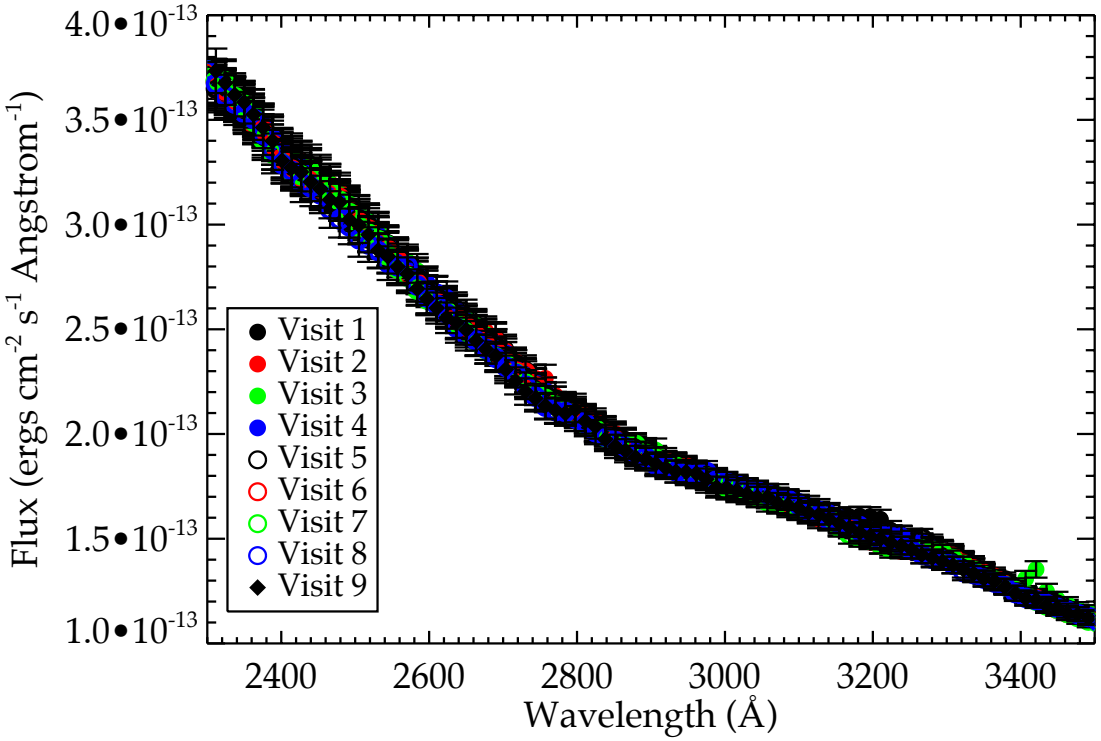

Figure 4: Similar plot to Figure 3, but for longer wavelength ranges. The fluxes at these wavelengths show no statistical evidence of change with time or among visits.

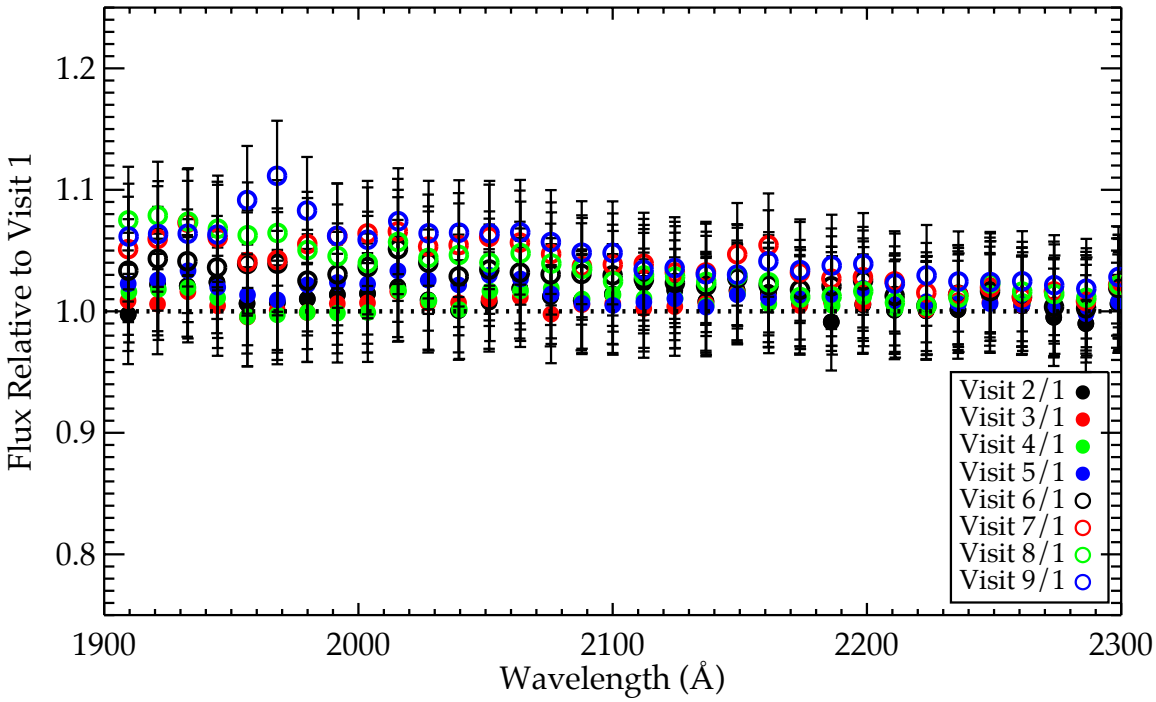

Figure 5: Shown here are the measured fluxes relative to Visit 1. Visually, the plot displays an increase in flux between visits at the bluest wavelengths. However, the change is not statistically significant.

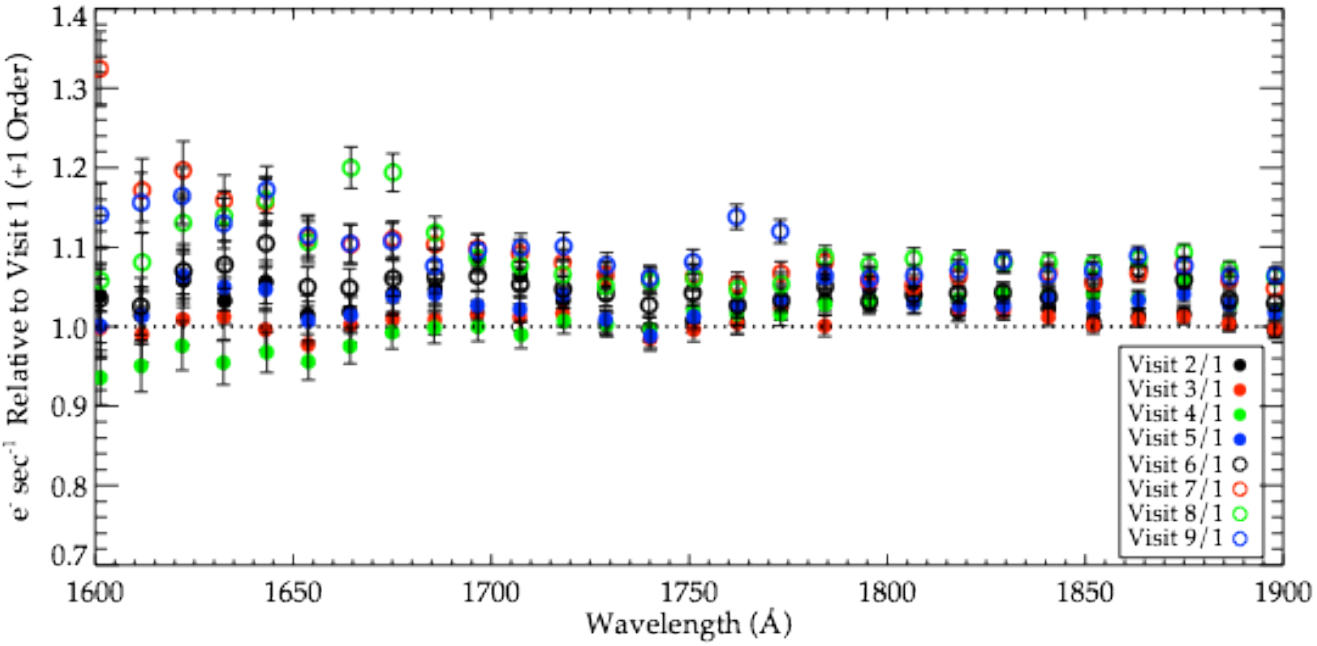

Figure 6: Similar to Figure 5, but *counts* are plotted relative to Visit 1 because the flux calibration at λ < 1900 Å is incomplete. The data are significantly noiser at these wavelengths but again, there is *slight* evidence of a change in the counts between vistis.

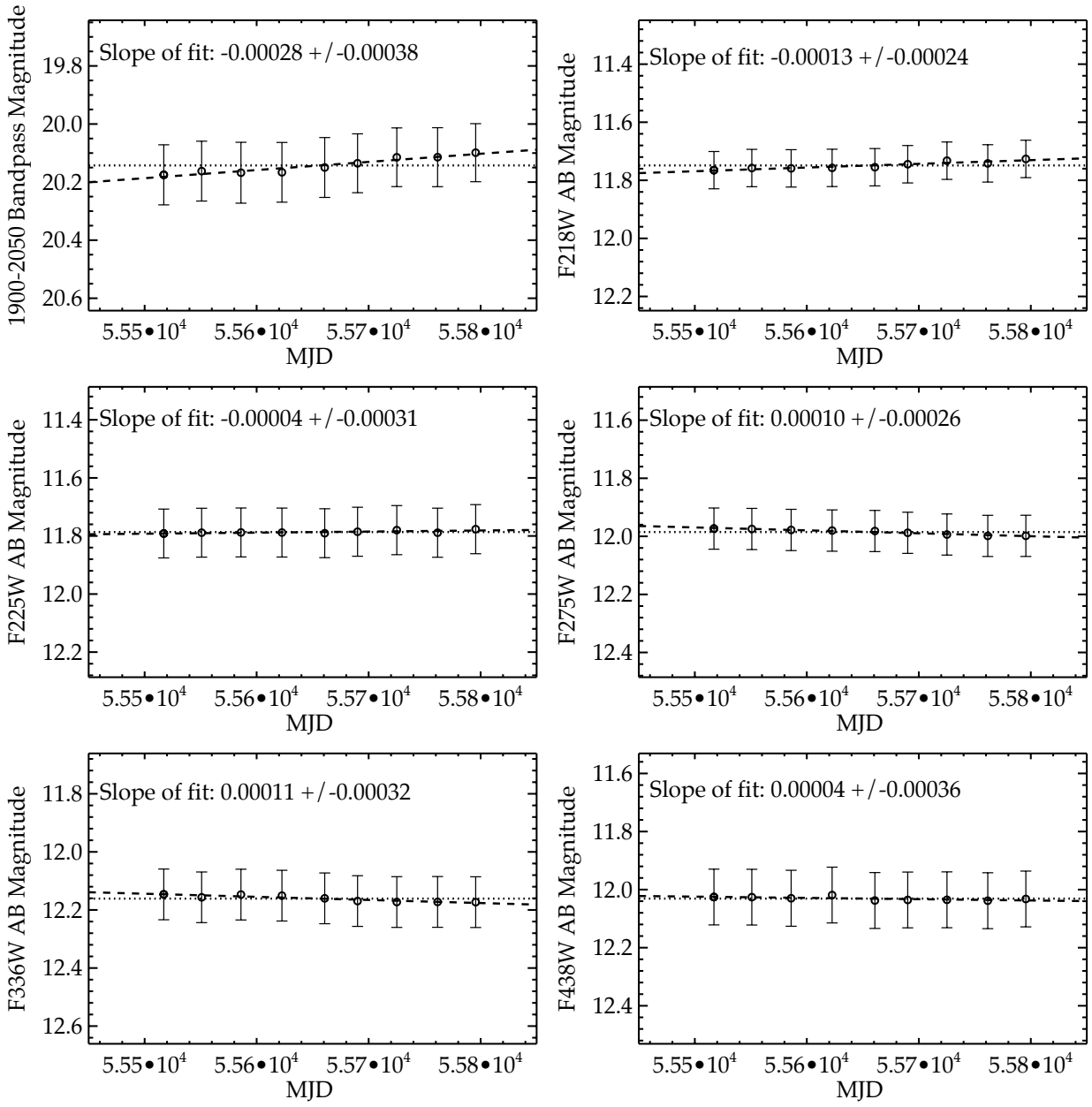

Figure 7: The G280 fluxes have been convolved with WFC3 filter transmission profiles and the appropriate PHOTPLAM values to obtain photometric magnitudes which can be directly compared with WFC3/UVIS photometry. A pseudo-filter has been created for monitoring changes as a function of time at wavelengths shorter than the bluest WFC3 imaging filter. Also shown are error-weighted least-squares fits to the data to test for evidence of change with time. Visually, the pesudo-filter appears to show an *increase* in flux with time, but not at a statistically significant level.

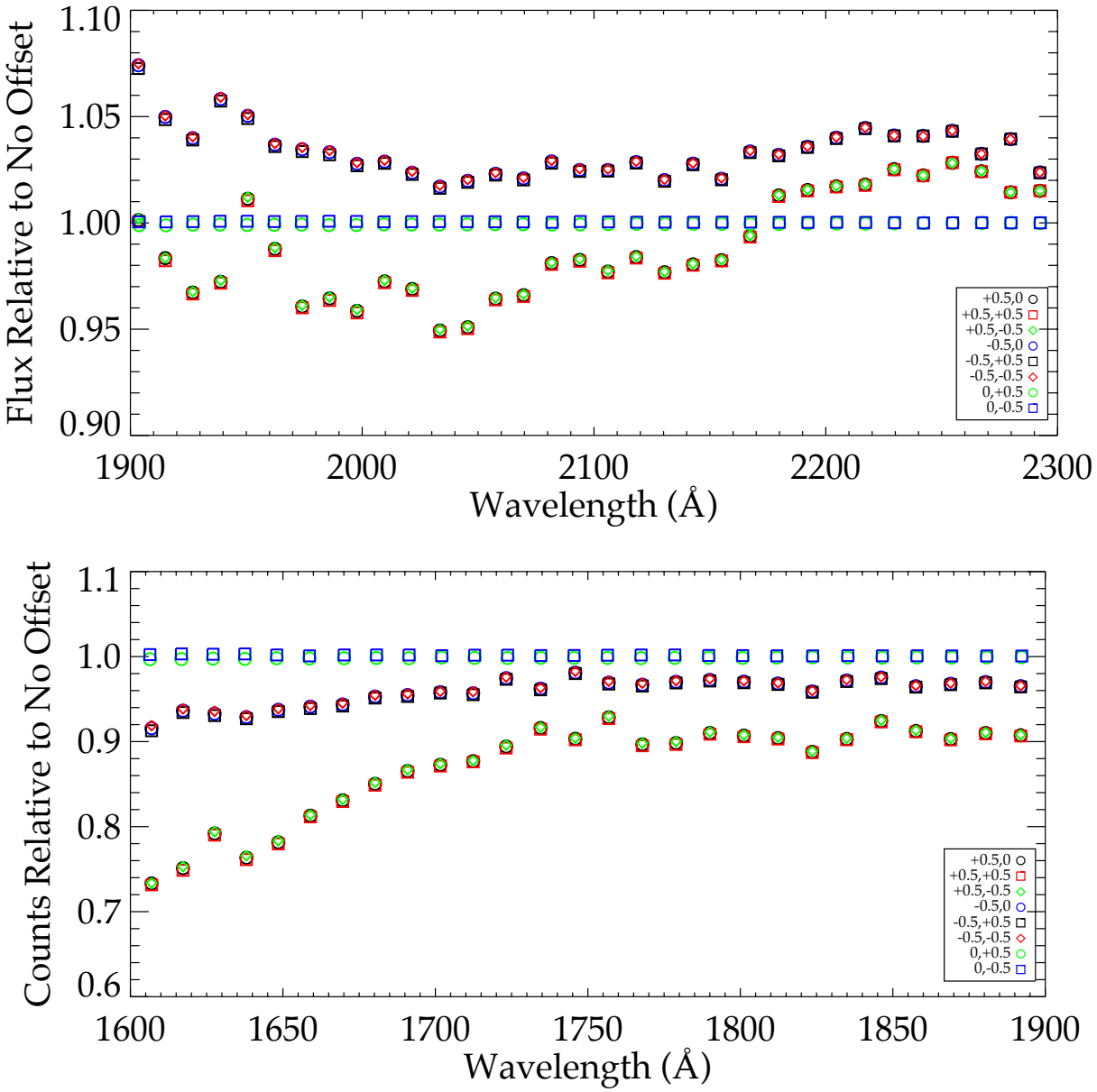

Figure 8: Demonstration of the additional errors introduced by an inaccurate object catalog. The plots show the relative differences in flux and native counts when +/-0.5 pix are added in X and Y to the coordinates of the standard star in the object catalog. All points are relative to fluxes and counts measured from the true position of the star (i.e. +0.5, 0 in the legend means the flux from a spectrum that was extracted using a catalog in which the true object coordinates were offset by that amount in pixels. The flux is thne relative to what it "should" be from an accurate object catalog). An offset in Y has a negligible impact, but +/- 0.5 pix in X can produce significant errors in the flux.